ACS OMEGA

http://pubs.acs.org/journal/acsodf

Article

Actuator Performance of Dielectric Elastomers Comprising Hydrogenated Carboxylated Acrylonitrile-Butadiene Rubber/Nitrile Group-Modified Titanium Oxide Particles

Ryosuke Matsuno, Yota Kokubo, Shigeaki Takamatsu, and Atsushi Takahara*

Cite This: *ACS Omega* 2021, 6, 6965−6972

Read Online

ACCESS | Metrics & More | Article Recommendations | Supporting Information

ABSTRACT: We prepared a dielectric elastomer actuator composed of hydrogenated carboxylated acrylonitrile-butadiene rubber (HXNBR)/nitrile group (CN)-modified and non-modified titanium oxide (TiO_2) particles with insulation properties. The CN group-containing silane coupling agent was synthesized via a thiol−ene reaction between acrylonitrile and 3-mercaptopropyltrimethoxysilane and immobilized onto the TiO_2 particle surface. The HXNBR/CN-modified and non-modified TiO_2 particle composite elastomer showed a high relative dielectric constant and generated stress in a low electric field. The relative dielectric constant increased proportionally with the amount of CN-modified TiO_2 particles, showing a value of 22 at 100 Hz. As the dielectric constant increased, the volumetric resistivity decreased; however, the dielectric breakdown strength was maintained at 95 V/mm. The generated stress of the composite elastomer increased in proportion to the relative dielectric constant, showing a maximum of 1.9 MPa. The card-house structure of TiO_2 particles in the composite elastomer is assumed to suppress the dielectric breakdown in a low electric field. Thus, we demonstrated that an elastomer containing a high dipole group on an insulating particle surface is capable of improving the power performance of soft actuators.

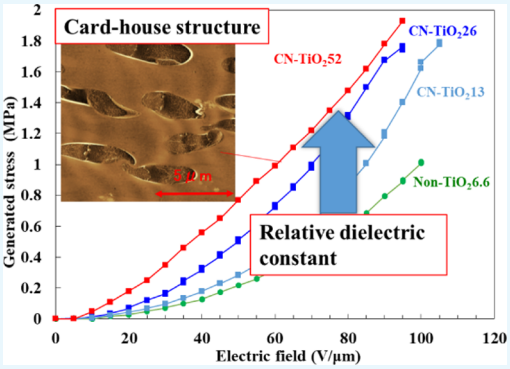

INTRODUCTION

A dielectric elastomer actuator (DEA), which has a sandwiched structure comprising a thin elastomer film and a compliant electrode, is a straightforward system compared to conventional hard actuators. When a voltage is applied to a DEA, the electrodes coated on both sides of the elastomer are pulled together, deforming the film in-between like artificial muscles.[1−5] The generated stress of the DEA is proportional to the dielectric constant according to the following effective compressive stress equation (eq 1)[1]

$$\sigma = \varepsilon_r \varepsilon_0 (V/d)^2 \quad (1)$$

where σ is the compressive stress, ε_r is the relative dielectric constant, ε_0 is the dielectric constant of vacuum, V is the driving voltage, and d is the thickness of the film.

To increase the generated stress, it is necessary to increase the relative dielectric constant (ε_r) or apply a high electric field (V/d). Various attempts to increase the relative dielectric constant have been made. The general approaches include the addition of ceramic particles with high dielectric constants,[6−10] addition of conductive nanofillers,[11,12] post-modification of polar groups in polymers,[13−17] and polymerization of highly polar monomers.[18−21] In composite elastomers with high dielectric constant particles, the approach of adding barium titanate ($BaTiO_3$) is often used; however, dielectric breakdown tends to occur in low electric fields. There is an intrinsic and an extrinsic origin for the dielectric breakdown. The intrinsic factor is an increase in the electrical conductivity because of a decrease in the volume resistivity caused by an increase in the dielectric constant. Extrinsic factors include the partial agglomeration of particles, presence of air voids, and incomplete interfaces between the polymer matrix and fillers during processing. These factors increase the leakage current and decrease the dielectric breakdown strength of the composites. Therefore, even with a high dielectric constant, they are prone to dielectric breakdown in low electric fields before high stresses can be generated. Composites containing conductive particles have the same problem. To avoid this problem, surface modification of $BaTiO_3$ particles has been reported.[22] However, since the surface of $BaTiO_3$ has no hydroxyl group, it is not easy to modify the surface by conventional coupling agents, such as silica (SiO_2) and titanium oxide (TiO_2). Furthermore, surface modification of

Received: December 22, 2020
Accepted: February 16, 2021
Published: March 4, 2021

Table 1. Amount Ratios Relative to HXNBR 100 phr and Properties of Dielectric Films Containing CN-Modified TiO_2, Non-modified TiO_2, and CN1

code	CN-modified TiO_2 (phr)	non-modified TiO_2 (phr)	CN-containing silane coupling agent (phr)	average relative dielectric constant at 100 Hz	average volume resistivity at 100 V (Ω·cm)	Young's modulus (MPa)
CN-$TiO_2$52	52	6.6		20.7	4.5×10^{11}	12.3
CN-$TiO_2$26	26	6.6		16.4	7.8×10^{11}	8.5
CN-$TiO_2$13	13	6.6		15.4	2.0×10^{12}	8.1
CN1-52			52	12.3	5.4×10^{11}	4.3
CN1-26			26	13.5	8.1×10^{11}	
CN1-13			13	10.5	7.5×10^{11}	
non-$TiO_2$6.6		6.6		12.6	3.6×10^{12}	6.7
HXNBR				13.9	8.9×10^{10}	

the high-dielectric constant particles reduces the relative dielectric constant of the composite.

On the other hand, the addition of insulating particles increases the insulating properties of the composite, allowing higher voltages to be applied. For high-voltage direct current (HVDC) cable development,[23] space-charge suppression is an important issue. Polymer electrical insulation materials capture charge carriers to generate space charges in a high electrical field, and the space charges induce serious distortions of the local electrical field, generating hot electrons and leading to electrical−mechanical energy storage and release.[24] The insulation effect of inorganic fillers such as SiO_2,[25] TiO_2,[26] zeolite,[27] ZnO,[28] and MgO[29,30] for space-charge suppression has been reported to improve the breakdown strength of HVDC cables. One of the proposed mechanisms is the trap potential model wherein nanofillers induce a large number of deep traps under high voltages, holding the injected carriers near the electrode and forming small amounts of homo-charges instead of large amounts of hetero-charges.[30] Therefore, the addition of insulating particles improves the breakdown strength of the actuator. However, as the dielectric constant of the elastomer does not increase, the generated stress in low electric fields does not increase. The high dielectric breakdown strength and the high relative dielectric constant are in a trade-off relationship, and it is difficult to achieve both.

In this study, we found that the dispersion states of surface-modified insulating particles could simultaneously improve the dielectric constant and dielectric breakdown. Hydrogenated carboxylated acrylonitrile-butadiene rubber (HXNBR) was selected as the matrix. In our previous study, HXNBR exhibited a high dielectric constant (~14.9) and flexibility[31] and was cross-linked by titanate.[32] TiO_2, which has an affinity for HXNBR, was selected as the insulating particle. To increase the dielectric constant, silane coupling agents with nitrile groups were synthesized and immobilized on the surface of the TiO_2 particles. We prepared a DEA composed of HXNBR/CN group-modified TiO_2 particles and evaluated its dielectric properties, electric properties, and performance.

RESULTS AND DISCUSSION

Dielectric Properties of Dielectric Elastomers. Table 1 summarizes the amount ratio and properties of dielectric films containing CN-modified TiO_2 (CN-TiO_2), non-modified TiO_2 (Non-TiO_2), and CN-containing silane coupling agent (CN1). Figure 1 shows the frequency dependence of the relative dielectric constant of the dielectric elastomers. The relative

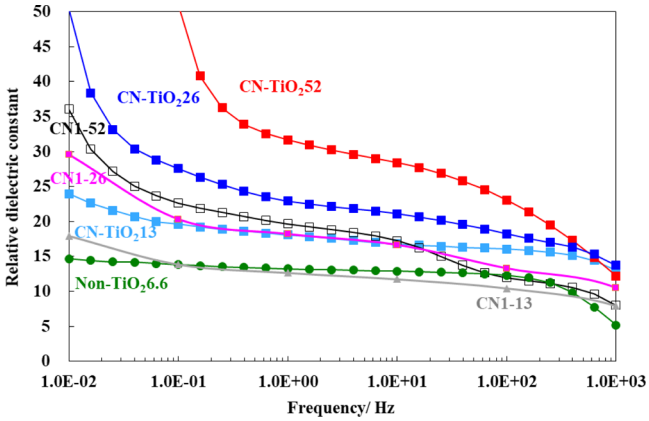

Figure 1. Frequency dependence of the relative dielectric constant of dielectric elastomers.

dielectric constant of the films with CN-TiO_2 and CN1 increased proportionally with the amount ratio in the measured frequency range of 1−100 Hz. Here, the values at frequencies below 1 Hz are not suitable for comparison because they are affected by interfacial polarization associated with the mobile charges between the particles and the matrix.[32,35,36] In addition, because the electrodes used do not have high conductivity, the conductivity decreased in some samples at frequencies above approximately 300 Hz and was not accurate. Therefore, 100 Hz was selected for comparison, and the relationship between the relative dielectric constant at 100 Hz and the amount ratio of CN-TiO_2 and CN1 is plotted in Figure 2. It was found that the dielectric constant of the dielectric elastomer containing CN-TiO_2 increased in

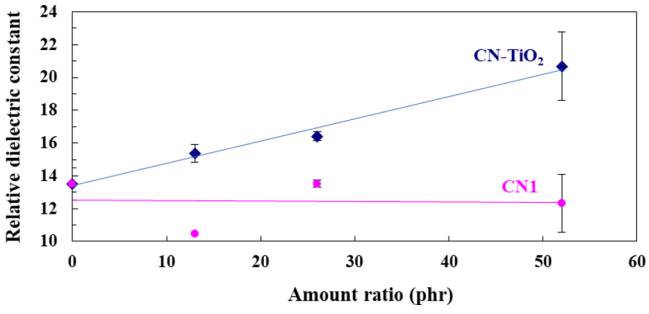

Figure 2. Relationship between the relative dielectric constant at 100 Hz and the amount ratio of CN-TiO_2 and CN1.

https://dx.doi.org/10.1021/acsomega.0c06219
ACS Omega 2021, 6, 6965−6972

proportion to the amount of CN-TiO_2, showing an average of 20.7 at an amount ratio of 52 phr, while that of the dielectric elastomer containing CN1 decreased slightly and then remained constant. At 1−10 Hz, the dielectric constant of CN1 increased slightly as the amount of CN1 increased but not as much as the dielectric constant of CN-TiO_2. This suggests that an electric field was effectively applied to the interface between HXNBR and the TiO_2 particle surface owing to the structure of nitrile groups concentrated at the interface.

Relationship of Volume Resistivity with the Amount Ratio of CN-TiO_2 and CN1 and with the Relative Dielectric Constant of Dielectric Elastomers. Figure 3

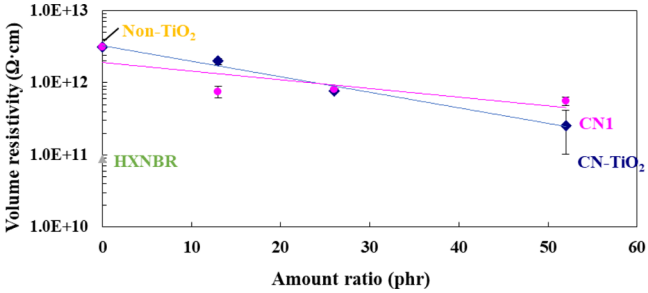

Figure 3. Relationship between the volume resistivity at 100 V and the amount ratio of CN-TiO_2 and CN1.

plots the relationship between the volume resistivity and the amount ratio of CN-TiO_2 and CN1. The volume resistivity of the elastomer containing Non-$TiO_2$6.6 was 3.6×10^{12} Ω·cm, which is the highest among the fabricated samples, while the volume resistivity of HXNBR alone was 8.9×10^{10} Ω·cm, indicating that the TiO_2 particles are insulating particles. The volume resistivity of the dielectric elastomer containing CN-TiO_2 decreased exponentially with the amount of CN-TiO_2, with a value of 4.5×10^{11} Ω·cm at 52 phr. The volume resistivity of the dielectric elastomers containing CN1 also decreased, but the decrease was smaller than that of CN-TiO_2. Figure 4 shows the relationship between the relative dielectric

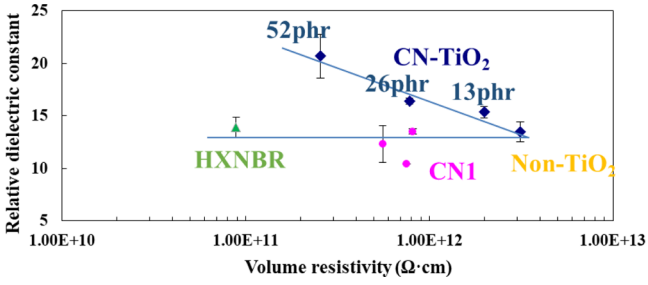

Figure 4. Relationship between the relative dielectric constant at 100 Hz and the volume resistivity of dielectric elastomers.

constant at 100 Hz and the volume resistivity of dielectric elastomers, which indicates that the dielectric constant and the volume resistivity of elastomers containing CN-TiO_2 are inversely related.

The theoretical relationship between the volume resistivity ρ and the relative dielectric constant ε is derived from the following equation

$$R \times C = \rho(d/S) \times \varepsilon(S/d) = \rho \times \varepsilon \quad (2)$$

where R is the electric resistance, C is the capacitance, d is the distance between the electrodes, and S is the area of the electrode. As shown in eq 2, the volume resistivity ρ and dielectric constant ε are theoretically inversely proportional. The volume resistivity correlates with the relative dielectric constant in the low-frequency region (0.01−1 Hz), as shown in Figure 1. The dielectric constant of Non-$TiO_2$6.6 with high volume resistivity does not increase in that frequency range. On the other hand, the dielectric constant of elastomers containing CN-TiO_2 and CN1 with low volume resistivity increase. Because the relative dielectric constant at low frequencies includes the movement of charge, it is considered that the charge generated by applying the voltage moves easily inside an elastomer with high relative permittivity, resulting in low volume resistivity. Thus, theoretically, it is difficult to simultaneously achieve a high dielectric constant and volume resistivity, and the trends in the measured values are consistent with the theoretical relations.

Actuator Performance. The actuator performance of the dielectric elastomers was evaluated. Figure 5 shows the

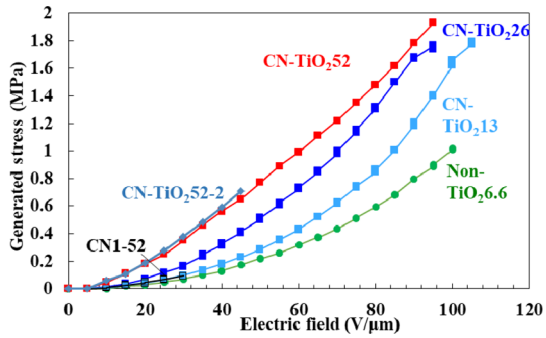

Figure 5. Generated stress of dielectric elastomers as a function of the electric field.

relationship between the generated stress and the electric fields. The elastomer containing Non-$TiO_2$6.6 with a high-volume resistivity of 3.6×10^{12} Ω·cm maintained integrity up to a dielectric breakdown strength of 100 V/μm. Elastomers including only CN1-52 with a volume resistivity of 5.4×10^{11} Ω·cm broke down at 30 V/μm. The high dielectric breakdown strength is presumed to be because of the insulation effect of TiO_2 and space-charge suppression. On the other hand, elastomers containing CN-TiO_2 with a volume resistivity of 4.5×10^{11} to 2.0×10^{12} Ω·cm did not break down up to an electric field of 95−105 V/μm, which is comparable to that of Non-$TiO_2$6.6. The maximum generated stress is nearly twice as high for CN-TiO_2 (1.7−1.9 MPa) as for Non-$TiO_2$6.6 (1.0 MPa). The plot shows that the generated stresses are proportional to the relative dielectric constant and the square of the electric field, as expressed in eq 1. It is obvious that the generated stress is proportional to the compressive stress. It was also found that the higher the relative dielectric constant of the elastomer, the higher the generated stress in the same electric field. In particular, the stresses generated by the actuator CN-$TiO_2$52, which has a large relative dielectric constant, were almost linearly proportional to the electric field. Therefore, the actuator can generate high stress in a low electric field, and the stress can be controlled by a linear proportional relationship with the electric field. However, CN-$TiO_2$52 sometimes suffered dielectric breakdown in a low electric field. CN-$TiO_2$52-2, which was prepared by the same method as that

https://dx.doi.org/10.1021/acsomega.0c06219
ACS Omega 2021, 6, 6965−6972

used for CN-$TiO_2$52, had dielectric breakdown in a low electric field of 45 V/μm. The dielectric breakdown strength varied even when prepared in the same way. The generated strain as a function of the electric field shown in Figure 6 was

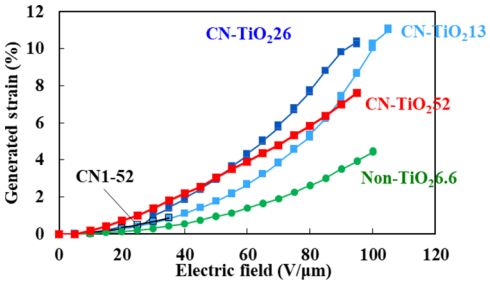

Figure 6. Generated strain of dielectric elastomers as a function of the electric field.

also proportional to the relative dielectric constant and the electric field, similar to the generated stress. However, because the elastomer containing CN-$TiO_2$52 has a high elastic modulus, the strain is smaller than those of CN-$TiO_2$26 and CN-$TiO_2$13 in a high electric field.

Dispersion State of Particles in Elastomers. In order to understand why dielectric breakdown does not occur in a low electric field even though the volume resistivity is low and why CN-$TiO_2$52 has a large variation in the dielectric breakdown strength, we observed the dispersion states of the particles in the elastomer. Figure 7 shows the dynamic force mode (DFM)

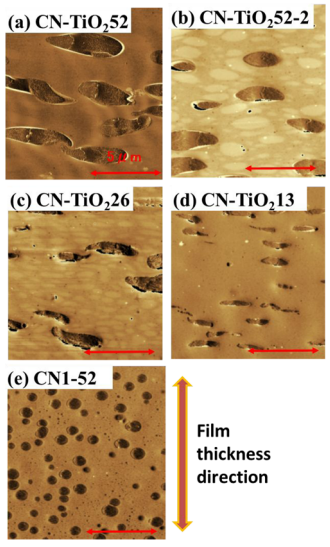

Figure 7. Cross section of elastomers: (a) CN-$TiO_2$52, (b) CN-$TiO_2$52-2, (c) CN-$TiO_2$26, (d) CN-$TiO_2$13, and (e) CN1-52. The scale bar is 5 μm.

images of the cross sections of elastomers. Interestingly, in the elastomer containing CN-TiO_2, the particles aggregated and assembled to form an elliptical shape in the direction perpendicular to the film thickness. As the amount of CN-TiO_2 added increased, the size of the aggregate increased. CN-$TiO_2$52, with a dielectric breakdown strength of 95 V/μm, had a larger particle aggregate size than that of CN-$TiO_2$52-2 with a dielectric breakdown strength of 45 V/μm. Thus, the card-house structure (Figure 8) is assumed to be responsible for the high dielectric breakdown strength despite the low volume

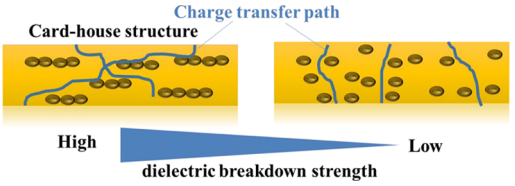

Figure 8. Schematic representation of the charge-transfer path.

resistivity. It has been reported that nanocomposites with layered silicates[37] and a mixture of nano-/microparticles[38] realized higher insulation breakdown strength. In a detailed observation of the discharge tree generated during the dielectric breakdown, it has been observed that many-branched discharge trees are generated in epoxy nanocomposites with dispersed layered silicate. It is believed that the densely and uniformly dispersed nanoparticles in the resin hinder the propagation of the discharge tree so that the propagation rate is slowed down because of the relaxation of the tip electric field of the individual branch by the surrounding tree, resulting in a longer breakdown time. Although it is unclear from this study whether the electrical tree is the primary cause of the dielectric breakdown, the card-house structure, similar to layered silicate, may be associated with a longer charge-transfer path, preventing the rapid transfer of charge. As a result, the breakdown strength of the elastomer, including CN-TiO_2, is thought to be high despite the low volume resistivity. Control of the shape of this aggregate is an issue for future research.

Comparison of Effective Compressive Stress of Dielectric Elastomers. The compressive stresses of the DEA fabricated in this study were compared with those of other samples. Table 2 summarizes the effective compressive stresses of various dielectric elastomers. The sample code provides the notation as mentioned in the respective references. They are not quantitative because the data were recorded for different elastomers and composites under different conditions but could be used for qualitative comparison. The HXNBR/CN-modified TiO_2 elastomer showed high effective compressive stress of 1.0−1.3 MPa at 1000 Hz and 1.3−1.7 MPa at 100 Hz compared to other elastomers (acrylic rubber, silicone rubber, and composite with $BaTiO_3$), except for the VHB 4910 acrylic (pre-strain 300, 300%). VHB 4910 acrylic with a planar pre-elongation of 300% exhibits an extremely high dielectric breakdown strength and therefore a high compressive stress. However, the value is in electric fields as high as 412 V/μm. Theoretically, according to eq 1, the compressive stress is proportional to the dielectric constant and the square of the electric field; therefore, acrylic and silicone rubber with insulating properties have higher maximum stress. Therefore, since the elastomers with $BaTiO_3$ have a high dielectric constant, they have a low dielectric breakdown strength, resulting in low compressive stress. Among the composites with $BaTiO_3$, the compressive stress and breakdown strength of NBR/BT-PCPA-KH570 were as high as 0.83 MPa and 75 V/μm, respectively. The high dielectric constant and dielectric breakdown strength to produce a high compressive stress is thought to be the combination of the NBR matrix with a high dielectric constant and surface-modification of $BaTiO_3$ by the co-deposited poly(catechol/polyamine) (PCPA) and γ-methacryloxypropyltrimethoxysilane (KH570). As a comparison, the compressive stress of 0.89 MPa in NBR/BT-PCPA-KH570 did not reach 1.3−1.7. MPa found in the HXNBR/CN-modified TiO_2

https://dx.doi.org/10.1021/acsomega.0c06219
ACS Omega 2021, 6, 6965−6972

Table 2. Comparison of Effective Compressive Stress of Dielectric Elastomers

code[a]	effective compressive stress (MPa)[b]	dielectric constant (1 kHz)[c]	dielectric breakdown strength (V/μm)[d]	reference
HXNBR/CN-$TiO_2$52 (25,0)	1.0	12.2	95	this work
	1.7 (100 Hz)	20.7 (100 Hz)		
HXNBR/CN-$TiO_2$26 (25,0)	1.1	13.7	95	this work
	1.3 (100 Hz)	16.4 (100 Hz)		
HXNBR/CN-TiO_{213} (25,0)	1.3	13.0	105	this work
	1.5 (100 Hz)	15.4 (100 Hz)		
CF19-2186 silicone (15,15)[e]	0.6	2.8	160	1
VHB 4910 acrylic (15,15)	0.13	4.8	55	1
VHB 4910 acrylic (300,300)	7.2	4.8	412	1
PDMS-$BaTiO_3$ 41 wt% (0,0)[f]	0.004	9.0	6.84	39
SR/m-BT10 wt % (0,0)[g]	0.013	10.48	12	8
NBR/BT-PCPA-KH570 50phr (0,0)[h]	0.83	16.65 (100 Hz)	75	22
silicone/BT 30phr (0,0)	0.10	3.85 (100 Hz)	55	7

[a]Pre-strain (x, y)%. [b]Estimated from eq 1. [c]Estimated from graphical data in the cited reference, when no tabulated values are provided. [d]Estimated from graphical data in the cited reference, when no tabulated values are provided. [e]CF19-2186 silicone is a general-purpose silicone that is made by mixing two components (polydimethylpolysiloxane is the main component). [f]PDMS is polydimethylpolysiloxane. [g]SR and BT are the slide ring and BaTiO3, respectively. [h]PCPA and KH570 are poly(catechol/polyamine) and γ-methacryloxypropyltrimethoxysilane, respectively.

elastomer. Although the results are partly influenced by the aggregation of particles, it was found that surface-modified insulating particles (TiO_2) with a high dielectric functional group (CN) result in a stronger power actuator than surface-modified highly dielectric particles ($BaTiO_3$) with a non-high dielectric functional group.

CONCLUSIONS

We prepared a DEA composed of HXNBR/CN-modified and non-modified TiO_2 with a high dielectric constant and high dielectric breakdown. The elastomer containing CN-$TiO_2$52 showed a high relative dielectric constant (maximum of 22 at 100 Hz) and generated stress (maximum of 1.9 MPa) at 95 V/mm, despite the theoretical decrease of volume resistivity with an increase in the dielectric constant. It is presumed that the card-house structure generated by the CN-modified and non-modified TiO_2 particles resulted in high dielectric constant and dielectric breakdown strength. The HXNBR/CN-modified TiO_2 elastomer actuator exhibited effective compressive stress of up to 1.7 MPa, more than twice the force of other elastomers. The elastomer containing high dipole groups on the insulating particle surface is capable of improving the power performance of soft actuators.

EXPERIMENTAL SECTION

Materials. Acrylonitrile, 3-mercaptopropyltrimethoxysilane, and diisopropylamine (DIPA) were purchased from Tokyo Chemical Industry Co., Ltd. (Japan). Acetylacetone (AcAc), isopropanol, methylethylketone (MEK), acetic acid, and methanol (super dehydrated) were purchased from FUJIFILM Wako Pure Chemical Corporation (Japan). A releasable film, PET3811, was obtained from Lintec Corporation (Japan). A PET film (Diafoil, Mitsubishi Chemical Corporation, Japan) was used as a finger contact prevention film for the electrode. HXNBR (Therban XT 8889; CN 33.8 mol %, COOH 3.8 mol %) was obtained from LANXESS (USA). Tetra-*i*-propoxy titanium (A-1) and tetrakis (2-ethylhexyloxy) titanium (TOT) 95% with 2-propanol (5%) were purchased from NIPPON SODA Co., Ltd. (Japan).

Synthesis of a Silane Coupling Agent with the CN Group via the Thiol−Ene Reaction. Figure 9 shows the scheme of immobilization of the CN group onto TiO_2 particles using a silane coupling agent. To increase the mobility of the polar group, the nitrile group is positioned at the end of the side chain. The thiol−ene addition reaction was used to introduce the CN group into the 3-mercaptopropyltrimethox-

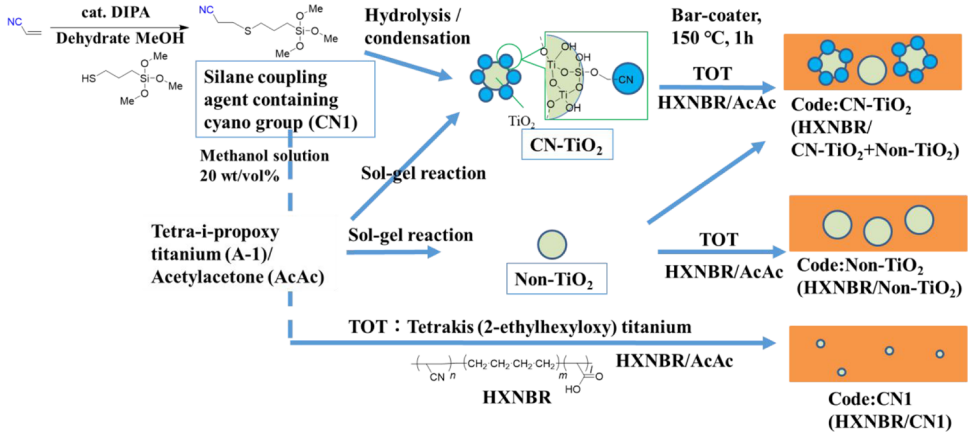

Figure 9. Schematic diagram of the synthesis of the silane coupling agent with a CN group (CN1), preparation of the CN group-modified TiO_2 particles (CN-TiO_2) and non-modified TiO_2 particles (Non-TiO_2), and preparation of dielectric elastomers (HXNBR/CN-TiO_2 + Non-TiO_2, HXNBR/Non-TiO_2, and HXNBR/CN1).

https://dx.doi.org/10.1021/acsomega.0c06219
ACS Omega 2021, 6, 6965−6972

ysilane coupling agent. The thiol−ene reaction is a click chemistry reaction[33,34] and is highly efficient for thiol addition. A weight of 5.3 g (0.10 mol) of acrylonitrile and 21.6 g (0.11 mol) of 3-mercaptopropyltrimethoxysilane were added to 70 mL of methanol (super dehydrated). To this methanol solution, 5 mol % DIPA with respect to silane was added as an amine catalyst, and the mixture was stirred at room temperature (25 ± 5 °C) overnight. The solvent was removed by evaporation under reduced pressure.

^{1}H NMR (400 MHz, MeOD): δ/ppm 0.75 (2H, $SiCH_2CH_2$), 1.68 (2H, $SiCH_2CH_2CH_2$), 2.55−2.79 (6H, $CNCH_2CH_2SCH_2$), 3.56 (OCH_3).

Immobilization of the CN Group onto TiO_2 Particles and HXNBR. The synthesized silane coupling agents were then immobilized on the surface of TiO_2 particles. First, a sol containing CN group-immobilized TiO_2 particles was prepared (Figure 9). The sol was then added to the HXNBR solution to form a dielectric elastomer composed of CN group-immobilized TiO_2 particles and an HXNBR matrix. TiO_2 particles were immobilized on HXNBR by their interaction with the carboxyl groups in HXNBR.

The details of the preparation of the dielectric elastomer are as follows: 0.01 mol of A-1 was added to 0.02 mol of AcAc. To this solution, prescribed weights (8, 16, and 32 g) of methanol solution containing CN1 20 wt/vol %, 5 mL (0.083 mol) of isopropanol, 10 mL (0.139 mol) of MEK, 0.03 mol of acetic acid, and 0.08 mol of pure water were added to obtain a sol of silane-containing TiO_2 particles. The sol was then aged at 40 °C for 2 h. The obtained sol was left at room temperature (25 ± 5 °C) overnight and then concentrated by an evaporator until the mass reduced to half. The median diameter of the TiO_2 particles was approximately 8 nm. In addition, non-modified TiO_2 particles were synthesized as a separate step. 0.01 mmol of A-1 was added to 0.02 mol of AcAc. To this solution, 5 mL (0.083 mol) of isopropanol, 10 mL (0.139 mol) of MEK, and 0.04 mol of pure water were added to obtain a sol of TiO_2 particles. The obtained sol was aged at 40 °C for 2 h. The median diameter was approximately 14 nm.

HXNBR was dissolved in AcAc at a concentration of 12 wt %. 100 phr of the polymer, prescribed phr (13, 26, and 52 phr in Table 1) of the CN group-modified TiO_2 sol, 6.6 phr of the non-modified TiO_2 sol, and 5 phr of AcAc solution containing 20 wt % TOT were mixed. After degassing, the solution was applied onto a releasable film, spread using a bar-coater, dried, and heated at 150 °C for 60 min. The thickness was approximately 22−39 μm.

As comparative samples, HXNBR/non-modified TiO_2 and HXNBR/CN1 composite films were prepared following the same steps, as shown in Figure 9. The amount ratios are listed in Table 1.

Characterization. The ^{1}H NMR spectra were recorded with a JNM-LA400 (JEOL Ltd., Japan) spectrometer. The relative dielectric constants at frequencies ranging from 0.01 to 1000 Hz (log sweep) were measured using a 1255B Frequency Response Analyzer and an impedance/gain-phase analyzer with a 1296A Interface (manufactured by Solartron Analytical, UK) and a sample holder (12962A). Theoretically, the relative dielectric constant is the real part of the complex dielectric constant, but in this study it is simply referred to as the relative dielectric constant. The generated stress was detected by a load cell attached to a tensile measurement device (EZ-S, Shimadzu Corporation., Japan) with a direct current high-pressure power supply (MAX-ELECTRONICS CO, Ltd., Japan). The Young's modulus was determined from the value when the pre-strain was set to 25% at the generated stress measurement. The cross-sectional view of the film was obtained using a scanning probe microscope SPM-9700 (Shimadzu Corporation, Japan) with an SI-DF40 cantilever in DFM. The cross section was prepared by microtoming with a glass knife at −80 °C after embedding the film in an epoxy resin. The volume resistivity was measured using a Digital Electrometer 8340A (ADC Corporation, Japan).

Sample Preparation for the Evaluation of Relative Dielectric Constant, Volume Resistivity, and Generated Stress and Strain. The sample preparation procedure for the evaluation of the relative dielectric constant, volume resistivity, and generated stress and strain is shown in the Supporting Information.

■ ASSOCIATED CONTENT

Supporting Information

The Supporting Information is available free of charge at https://pubs.acs.org/doi/10.1021/acsomega.0c06219.

> Sample preparation for the measurement of relative dielectric constant and volume resistivity on the composite elastomer, sample setting and measurement of the generated stress and strain, generated strain of dielectric elastomers as a function of the electric fields, Fourier-transform infrared spectra of CN-TiO_2 particles, and frequency dependence of the relative dielectric loss of dielectric elastomers (PDF)

■ AUTHOR INFORMATION

Corresponding Author

Atsushi Takahara − *Institute for Materials Chemistry and Engineering, Kyushu University, Fukuoka 819-0395, Japan;* orcid.org/0000-0002-0584-1525; Email: takahara@cstf.kyushu-u.ac.jp

Authors

Ryosuke Matsuno − *KOINE Project Division, Global Innovation Center (GIC) and Institute for Materials Chemistry and Engineering, Kyushu University, Kasuga, Fukuoka 816-8580, Japan*

Yota Kokubo − *Sumitomo Riko Company Limited, Komaki-shi, Aichi 485-8550, Japan*

Shigeaki Takamatsu − *Sumitomo Riko Company Limited, Komaki-shi, Aichi 485-8550, Japan*

Complete contact information is available at: https://pubs.acs.org/10.1021/acsomega.0c06219

Notes

The authors declare no competing financial interest.

■ ACKNOWLEDGMENTS

This research was supported by the Adaptable and Seamless Technology Transfer Program through Target-driven R&D (A-STEP, AS2525027M) from Japan Science and Technology Agency (JST). We are grateful to Dr. Kazunobu Hashimoto from former Sumitomo Riko Company and A-STEP member for contribution to the establishment of research system. NMR measurements were supported by Evaluation Center of Materials Properties and Function, Institute for Materials Chemistry and Engineering, Kyushu University. This work was the result of using research equipment shared in the MEXT

Project for promoting public utilization of advanced research infrastructure (program for supporting the introduction of the new sharing system) grant number JPMXS0422300120.

REFERENCES

(1) Pelrine, R.; Kornbluh, R.; Pei, Q.; Joseph, J. High-speed electrically actuated elastomers with strain greater than 100%. *Science* **2000**, *287*, 836−839.
(2) Michel, S.; Zhang, X. Q.; Wissler, M.; Löwe, C.; Kovacs, G. A Comparison Between Silicone and Acrylic Elastomers as Dielectric Materials in Electroactive Polymer Actuators. *Polym. Int.* **2009**, *59*, 391−399.
(3) Biggs, J.; Danielmeier, K.; Hitzbleck, J.; Krause, J.; Kridl, T.; Nowak, S.; Orselli, E.; Quan, X.; Schapeler, D.; Sutherland, W.; Wagner, J. Electroactive Polymers: Developments of and Perspectives for Dielectric Elastomers. *Angew. Chem., Int. Ed.* **2013**, *52*, 9409−9421.
(4) Madsen, F. B.; Daugaard, A. E.; Hvilsted, S.; Skov, A. L. The Current State of Silicone-Based Dielectric Elastomer Transducers. *Macromol. Rapid Commun.* **2016**, *37*, 378−413.
(5) Pelrine, R.; Kornbluh, R.; Joseph, J.; Heydt, R.; Pei, Q.; Chiba, S. High-Field Deformation of Elastomeric Dielectrics for Actuators. *Mater. Sci. Eng., C* **2000**, *11*, 89−100.
(6) Huang, X.; Xie, L. Y.; Hu, Z. W.; Jiang, P. K. Influence of $BaTiO_3$ Nanoparticles on Dielectric, Thermophysical and Mechanical Properties of Ethylene-Vinyl Acetate Elastomer/$BaTiO_3$ Microcomposites. *IEEE Trans. Dielectr. Electr. Insul.* **2011**, *18*, 375−383.
(7) Yang, D.; Huang, S.; Ruan, M.; Li, S.; Wu, Y.; Guo, W.; Zhang, L. Improved electromechanical properties of silicone dielectric elastomer composites by tuning molecular flexibility. *Compos. Sci. Technol.* **2018**, *155*, 160−168.
(8) Yang, D.; Ge, F.; Tian, M.; Ning, N.; Zhang, L.; Zhao, C.; Ito, K.; Nishi, T.; Wang, H.; Luan, Y. Dielectric elastomer actuator with excellent electromechanical performance using slide-ring materials/barium titanate composites. *J. Mater. Chem. A* **2015**, *3*, 9468−9479.
(9) Yu, K.; Niu, Y. J.; Bai, Y. Y.; Zhou, Y. C.; Wang, H. Poly(vinylidene fluoride) polymer based nanocomposites with significantly reduced energy loss by filling with core-shell structured $BaTiO_3/SiO_2$ nanoparticles. *Appl. Phys. Lett.* **2013**, *102*, 102903.
(10) Yu, K.; Wang, H.; Zhou, Y.; Bai, Y.; Niu, Y. Enhanced dielectric properties of Ba TiO_3/poly(vinylidene fluoride) nanocomposites for energy storage applications. *J. Appl. Phys.* **2013**, *113*, 034105.
(11) Hu, W.; Zhang, S. N.; Niu, X.; Liu, C.; Pei, Q. An aluminum nanoparticle-acrylate copolymer nanocomposite as a dielectric elastomer with a high dielectric constant. *J. Mater. Chem. C* **2014**, *2*, 1658−1666.
(12) Poikelispää, M.; Shakun, A.; Das, A.; Vuorinen, J. Improvement of actuation performance of dielectric elastomers by barium titanate and carbon black fillers. *J. Appl. Polym. Sci.* **2016**, *133*, 44116.
(13) Kim, J. Y.; Park, S. H.; Yu, S. Effect of chlorine-containing polymer additive on dielectric performance of polymer dielectric films. *Electron. Lett.* **2014**, *50*, 357−358.
(14) Zhang, L.; et al. Highly improved electro-actuation of dielectric elastomers by molecular grafting of azobenzenes to silicon rubber. *J. Mater. Chem. C* **2015**, *3*, 4883−4889.
(15) Inutsuka, M.; Inoue, K.; Hayashi, Y.; Inomata, A.; Sakai, Y.; Yokoyama, H.; Ito, K. Highly dielectric and flexible polyrotaxane elastomer by introduction of cyano groups. *Polymer* **2015**, *59*, 10−15.
(16) Tasaka, S.; Inagaki, N.; Miyata, S.; Chiba, T. Electrical properties of cyanoethylated polysaccharides. *Sen'i Gakkaishi* **1988**, *44*, 546−550.
(17) Kinpara, S.; Tasaka, S.; Inagaki, N. Molecular Motion and Dielectricity in Polymers with Cyanoethyl Group. *Sen'i Gakkaishi* **1993**, *49*, 6−11.
(18) Tasaka, S.; Inagaki, N.; Okutani, T.; Miyata, S. Structure and properties of amorphous piezoelectric vinylidene cyanide copolymers. *Polymer* **1989**, *30*, 1639−1642.
(19) Tasaka, S.; Nakamura, T.; Inagaki, N. Ferroelectric Behavior in Copolymers of Acrylonitrile and Allylcyanide. *Jpn. J. Appl. Phys.* **1992**, *31*, 2492−2494.
(20) Wei, J.; Zhang, Z.; Tseng, J.-K.; Treufeld, I.; Liu, X.; Litt, M. H.; Zhu, L. Achieving High Dielectric Constant and Low Loss Property in a Dipolar Glass Polymer Containing Strongly Dipolar and Small-Sized Sulfone Groups. *ACS Appl. Mater. Interfaces* **2015**, *7*, 5248−5257.
(21) Zhu, Y.-F.; Zhang, Z.; Litt, M. H.; Zhu, L. High Dielectric Constant Sulfonyl-Containing Dipolar Glass Polymers with Enhanced Orientational Polarization. *Macromolecules* **2018**, *51*, 6257−6266.
(22) Yang, D.; Ni, Y.; Xu, Y.; Kong, X.; Feng, Y.; Zhang, L. Nitrile-butadiene rubber composites with improved electromechanical properties obtained by modification of $BaTiO_3$ with co-deposited catechol/polyamine and silane grafting. *Polymer* **2019**, *183*, 121813.
(23) Hanley, T. L.; Burford, R. P.; Fleming, R. J.; Barber, K. W. A general review of polymeric insulation for use in HVDC cables. *IEEE Electr. Insul. M.* **2003**, *19*, 13−24.
(24) Mazzanti, G.; Montanari, G. C.; Dissado, L. A. Electrical aging and life models: The role of space charge. *IEEE Trans. Dielectr. Electr. Insul.* **2005**, *12*, 876−890.
(25) Zhang, L.; Khani, M. M.; Krentz, T. M.; Huang, Y.; Zhou, Y.; Benicewicz, B. C.; Nelson, J. K.; Schadler, L. S. Suppression of space charge in crosslinked polyethylene filled with poly(stearyl methacrylate)-grafted SiO_2 nanoparticles. *Appl. Phys. Lett.* **2017**, *110*, 132903.
(26) Zha, J.-W.; Dang, Z.-M.; Song, H.-T.; Yin, Y.; Chen, G. Dielectric properties and effect of electrical aging on space charge accumulation in polyimide/TiO2 nanocomposite films. *J. Appl. Phys.* **2010**, *108*, 094113.
(27) Han, B.; Wang, X.; Sun, Z.; Yang, J.; Lei, Q. Space charge suppression induced by deep traps in polyethylene/zeolite nanocomposite. *Appl. Phys. Lett.* **2013**, *102*, 012902.
(28) Tian, F.; Lei, Q.; Wang, X.; Wang, Y. Effect of deep trapping states on space charge suppression in polyethylene/ZnO nanocomposite. *Appl. Phys. Lett.* **2011**, *99*, 142903.
(29) Peng, S.; He, J.; Hu, J.; Huang, X.; Jiang, P. Influence of Functionalized MgO Nanoparticles on Electrical Properties of Polyethylene Nanocomposites. *IEEE Trans. Dielectr. Electr. Insul.* **2015**, *22*, 1512−1519.
(30) Takada, T.; Hayase, Y.; Tanaka, Y.; Okamoto, T. Space charge trapping in electrical potential well caused by permanent and induced dipoles for LDPE/MgO nanocomposite. *IEEE Trans. Dielectr. Electr. Insul.* **2008**, *15*, 152−160.
(31) Matsuno, R.; Takagaki, Y.; Ito, T.; Yoshikawa, H.; Takamatsu, S.; Takahara, A. Relationship between the Relative Dielectric Constant and the Monomer Sequence of Acrylonitrile in Rubber. *ACS Omega* **2020**, *5*, 16255−16262.
(32) Matsuno, R.; Kokubo, Y.; Kumagai, S.; Takamatsu, S.; Hashimoto, K.; Takahara, A. Molecular Design and Characterization of Ionic Monomers with Varying Ion Pair Interaction Energies. *Macromolecules* **2020**, *53*, 1629−1637.
(33) Hoyle, C. E.; Bowman, C. N. Thiol-Ene Click Chemistry. *Angew. Chem., Int. Ed.* **2010**, *49*, 1540−1573.
(34) Matsuno, R.; Takami, K.; Ishihara, K. Simple Synthesis of a Library of Zwitterionic Surfactants via Michael-Type Addition of Methacrylate and Alkane Thiol Compounds. *Langmuir* **2010**, *26*, 13028−13032.
(35) Zhu, L. Exploring Strategies for High Dielectric Constant and Low Loss Polymer Dielectrics. *J. Phys. Chem. Lett.* **2014**, *5*, 3677−3687.
(36) Xia, W.; Zhang, Z. PVDF-based dielectric polymers and their applications in electronic materials. *IET Nanodielectr.* **2018**, *1*, 17−31.
(37) Imai, T.; Sawa, F.; Ozaki, T.; Nakano, T.; Shimizu, T.; Yoshimitsu, T. Preparation and Insulation Properties of Epoxy-Layered Silicate Nanocomposite. *IEEJ Trans. Fundam. Mater.* **2004**, *124*, 1065−1072.
(38) Imai, T.; Sawa, F.; Nakano, T.; Ozaki, T.; Shimizu, T.; Kozako, M.; Tanaka, T.; Tanaka, T. Effects of Nano- and Micro-filler Mixture

https://dx.doi.org/10.1021/acsomega.0c06219
ACS Omega 2021, 6, 6965−6972

on Electrical Insulation Properties of Epoxy Based Composites. *IEEE Trans. Dielectr. Electr. Insul.* **2006**, *13*, 319−326.
(39) Nayak, S.; Chaki, T. K.; Khastgir, D. Development of Flexible Piezoelectric Poly(dimethylsiloxane)-$BaTiO_3$ Nanocomposites for Electrical Energy Harvesting. *Ind. Eng. Chem. Res.* **2014**, *53* (39), 14982−14992.

https://dx.doi.org/10.1021/acsomega.0c06219
ACS Omega 2021, 6, 6965−6972